PHYSICAL REVIEW B VOLUME 23, NUMBER 6 15 MARCH 1981

Magnetothermal oscillations, Fermi surface, and band structure of lowest-stage nitric-acid–graphite intercalation compounds

Ch. Simon, F. Batallan, and I. Rosenman
Groupe de Physique des Solides de l'Ecole Normale Supérieure, Université Paris 7, Tour 23, 2 Place Jussieu, 75221 Paris Cedex 05, France*

H. Fuzellier
Laboratoire de Chimie Minérale Appliquée, Université de Nancy I, 54037 Nancy Cedex, France*
(Received 4 March 1980)

Results on quantum magnetothermal oscillations in graphite acceptor compounds, C_{8s} (HNO_3) $s = 2,3,4$ are presented, including de Haas–van Alphen frequencies and effective masses. The frequency spectrum is different for every stage. Combination frequencies are present in every case and are attributed to magnetic breakdown. The interpretation is based on and confirms the independent two-dimensional zone model of the graphite acceptor compounds. A combination of the band-structure calculation of Blinowski and Rigaux and the folding of these bands in the Brillouin zone of the intercalate compound is used. This gives good agreement for the Fermi surfaces and the effective masses. Numerical values are given for the band parameters. Extra parameters are introduced in order to explain the results. For the second stage a charge-transfer ratio of $f = 0.6$ and a Fermi-level shift of 1.08 eV are found. For the third stage 99% of the excess charge is localized in the carbon layer adjacent to the intercalate. The electrostatic energy difference between this layer and the inner one is found to be $2\epsilon = 1.4$ eV.

I. INTRODUCTION

The graphite acceptor compounds (GAC) obtained by the intercalation of various molecules such as halogens or acids in graphite have two remarkable properties: a metallic character in the layer planes and a very large anisotropy. The metallic character is shown by the presence of a deep plasma edge in the optical reflectivity[1] as well as by the linear variation of the in-plane resistivity versus the temperature T in the room-temperature domain.[2] The latter fact is consistent with scattering by acoustic phonons. At lower temperatures a T^2 variation has been claimed[3] which should be related to the 2D Fermi surface (FS) (Ref. 4) of the GAC that we have proposed.[5,6] At still lower temperatures the electrical conductivity saturates as is expected in a metal from scattering by static defects.

If one compares the GAC with pristine graphite, a double aspect has to be mentioned. The intercalation of an acceptor molecule not only increases strongly the in-plane electrical conductivity [up to a factor of 20 for AsF_5 (Ref. 7)] as can be expected from the enhancement of the carrier density, but at the same time the c-axis conductivity is strongly lowered [up to a factor of 50 for AsF_5 (Ref. 7)]. This gives in the conductivity a very large anisotropy, e.g., 2.7×10^6 for AsF_5 at room temperature which is 10^3 times the anisotropy of graphite.

The origin of the special electronic properties of the GAC is the charge transfer which occurs between the graphite and the intercalate during the intercalation process, in which electrons are transferred from the graphite to the intercalate leaving holes in the graphite layers. The number of carriers transferred is characterized by the charge-transfer ratio f, defined as the fraction of the intercalate molecules which are ionized, $f=1$ meaning total ionization. For the nitric acid which accepts a maximum of one electron per molecule the number of electrons transferred by the HNO_3 molecule is f; but for the bromine molecule which can accept a maximum of two electrons this number is $2f$. Although the parameter f is very important, it is difficult to measure, and widely dispersed values have been given in the literature. For example, estimates of f between 0.01 and 1 have been given for the bromine GAC.[8] The origin of these discrepancies is the lack of methods for direct determination of f, the estimates depending on the model used to interpret the experimental results. However, recent results use 2D models for the GAC and give a rather realistic value of f. Weinberger *et al.*[9] have measured the magnetic spin susceptibility of $C_{8s}AsF_5$ by electronic and nuclear magnetic resonance. From the value of the density of states at the Fermi energy they have deduced $f=0.24$ for the first stage and $f=0.48$ for the second stage. Rosenman *et al.*[6] have proposed for the dilute Br_2 GAC a value of $f=0.5$, obtained from the study of magnetothermal oscillations using a 2D Fermi-surface model. More recently Blinowski *et al.*[10] interpreted their optical reflectivity experiments with a 2D model made of s graphite interacting layers differently charged. They found for second-stage compounds values of f from 0.3 to 0.5.

Another aspect of the charge transfer is the distribution of the holes among the different graphite layers. This problem is closely related to the electronic structure of the GAC. The first model proposed for the electronic structure of the GAC was the rigid-band model (RBM) of Dresselhaus *et al.*,[11] based on the 3D bands of pure graphite. In this approach the only effect of the intercalation is to shift the Fermi level according to the density of carriers. This model implies a uniform charge distribution in the sample. One of its consequences is that the FS of the GAC should vary continuously as a function of the intercalate concentration. We have shown[6] in the dilute bromine GAC that this is not the case, as the de Haas–van Alphen (dHvA) frequencies are independent of the intercalate concentration. This result rules out the 3D RBM and means that in a GAC the carbon layers are differently charged by the free carriers and give different contributions to the electrical conductivity.[12] The first authors to draw attention to screening effects were Spain and Nagel[12] who estimated the screening length along the c axis from the value of the Fermi vector in pure graphite. They found $\lambda = 5$ Å. Batallan *et al.*[5,6] proposed complete charge screening between the carbon layer adjacent to the intercalate and the next carbon layer, using a 2D FS in order to explain their results. A numerical estimate[6] in the case of Br_2 gives an upper limit of 1 Å for the screening length. Pietronero *et al.*[13] computed the screening effects within the Thomas-Fermi approximation and found that the charge density falls by one order of magnitude between the adjacent carbon layer and the next carbon layer. Shieh *et al.*[14] have studied the optical reflectivity in the HNO_3 GAC. They have found that there is no Burstein-Moss shift within the second-nearest carbon layer. This means a complete screening by the two adjacent carbon layers.

It is very important to take into account the screening effects in the determination of the electronic structure of the GAC. Rosenman *et al.*[6] have recently proposed a very simple model for the electronic structure of the "dilute" GAC: the modulated electronic structure (MES). The MES was based on the results of magnetothermal oscillations (MTO) in dilute bromine GAC. They have found that in this case the FS is independent of the intercalate concentration: the FS includes that of 3D graphite and a new 2D FS. The MES is thus composed of an alternating sequence of zones of low and high free-carrier density. They have defined the latter as a 2D metallic sandwich (MS) made up of the intercalate layer and the two adjacent carbon layers. The 2D MS was described within the nearly-free-electron (NFE) approximation. This made it possible to explain most of the dHvA frequencies when the effects of magnetic breakdown of the primitive NFE orbits were included. The remaining frequencies were explained by the presence of an incommensurable charge-density wave stabilized by the saddle points in the 2D FS.[15]

In this paper we present a detailed study of the MTO in the low stages of nitric acid GAC. We have investigated stages 2, 3, and 4 of the residual variety of HNO_3 GAC (Ref. 16) in order to study the electronic structure of the low-stage GAC's.

To understand our results we must take into account not only the adjacent carbon layers but also other carbon layers surrounding the intercalate. A brief report of the experimental results has been given elsewhere.[17,18]

Section II describes the HNO_3 GAC and some of their properties. In Sec. III we present the experimental technique. Section IV is devoted to the results. In Sec. V we discuss some general aspects of these results. In Sec. VI we describe a 2D model of the electronic structure of the GAC. In Sec. VII we give a detailed discussion of the second-stage GAC and we give numerical values for the band parameters of the FS and effective masses; we also extend the model of Blinowski and Rigaux in order to introduce new coupling parameters neglected by these authors. In Sec. VIII we briefly discuss our results for stages 3 and 4. Section IX is devoted to the conclusion.

II. GRAPHITE NITRATES

Two varieties of graphite nitrates[16] exist:

The normal graphite nitrates (NGN) of composition $C_{5s}HNO_3$ and of stages $s = 1, 2, 3, 4, \ldots$. Their interplanar distance is 7.80 Å.

The "residual" graphite nitrates (RGN) of composition $C_{8s}HNO_3$ and of stages $s = 2, 3, 4, \ldots$. Their interplanar distance 6.55 Å is smaller than that of the NGN from which they are obtained.

The NGN are prepared by the method of the "two-boules tube" by intercalating the HNO_3 in vapor phase. The different stages are obtained by monitoring the intercalation with *in situ* x-ray diffraction. The graphite is maintained at room temperature whereas the nitric acid, which defines the vapor pressure in the tube, is at a temperature between −20 °C and 20 °C. The NGN are then placed under a current of dry air or nitrogen for a week at room temperature, resulting in the RGN. The samples are controlled by measuring the mass, the thickness, and the electrical resistivity as well as by x rays. The RGN are particularly stable at room temperature (for at least

several months). This has been checked both by x rays and by the study of MTO where we have found exactly the same results after several months on the same samples. The samples that we use are thin discs, of $\phi \approx 4$ mm and a thickness of 0.2 mm, of highly oriented pyrolytic graphite (HOPG).

We studied five different RGN samples: two of stage 2, one of stage 3, and two of stage 4. The mass of the samples was in the range of 3 to 4 mg.

III. EXPERIMENTAL ASPECTS

A. Magnetothermal oscillations

The magnetothermal oscillations (MTO) are quantum oscillations of the temperature versus the magnetic field in a metallic sample at low temperature and high magnetic field under adiabatic conditions. The origin of these oscillations is the quantization of the electron gas in Landau levels in the presence of a magnetic field.

The MTO are given by the formula[19]

$$\delta T = \sum_{i,n} D_{i,n}(T, B, \theta) \sin \frac{2\pi F_i(\theta)}{B} , \tag{3.1}$$

where δT is the oscillatory part of the temperature T, B the magnetic field, θ the angle between the c axis of the sample and the magnetic field, and F_i the dHvA frequency. This frequency is related to the extremal cross section of the FS perpendicular to B by the Onsager relation

$$F_i(\theta) = \frac{\hbar}{2\pi e} A_i(\theta) . \tag{3.2}$$

There are as many values of i as extremal cross sections in the FS. As in the well-known dHvA effect, harmonic frequencies nF_i are also present. The amplitude of the oscillations corresponding to a given FS cross section is given by the formula

$$D_{i,n}(T, B, \theta) = D_n \frac{T}{C_B(T)} \left(\frac{\partial^2 A_i(\theta)}{\partial k_z^2} \right)^{-1/2} \times \exp\left(\frac{-\lambda n m_i(\theta) T_i}{B} \right) L\left(\frac{\lambda n m_i(\theta) T}{B} \right) , \tag{3.3}$$

where $C_B(T)$ is the specific heat of the sample, m_i the effective mass in units of free-electron mass m_0, T_i the Dingle temperature, λ a numerical constant, $\lambda = 14.69$ tesla/K, and

$$L(x) = \frac{x \cosh x - \sinh x}{\sinh^2 x} . \tag{3.4}$$

The Dingle temperature T_i is related to the average orbital relaxation time τ_i by

$$T_i = \hbar / 2\pi k_B \tau_i . \tag{3.5}$$

As is shown in (3.3) the apparent effective mass corresponding to nF_i is nm_i.

We use the MTO as a spectroscopic technique. The dHvA frequencies give the extremal cross sections of the FS. The effective masses and the Dingle temperature are obtained from the variation of the amplitude D_i versus the magnetic field and the temperature, according to formula (3.3). From the angular variation, one determines the shape of the FS.

B. Experimental setup

We have used standard low-frequency field modulation[20] at 11.1 Hz to measure the MTO. The main field was produced by an 80-kOe superconducting coil and was varied such that $1/B$ was proportional to time. Temperatures down to 1 K can be obtained. Thermometers of the type described by McCombe and Seidel[21] were used. They were made of slices of Allen Bradley $\frac{1}{10}$-W 6.2-kΩ resistors. These discs of $\phi \approx 1.5$ mm were carefully polished to a thickness of 0.2 mm and then gold-plated by evaporation. The current leads were made of $\frac{2}{100}$-mm diameter Constantan wire and attached to the discs by gold paint. The thermometers were glued by silicon grease to a small plate (0.15 mm thick) of quartz, a very good thermal conductor at liquid-helium temperatures. The quartz was glued with GE 7031 varnish to the top of a hollow graphite column which served as a thermal insulator and was mounted on a fixed or rotating sample holder. The samples were glued by Voltalef[22] grease to the quartz plate. The whole system was in loose thermal contact with the pumped helium liquid by introducing helium gas (0.1 to 0.01 Torr) in the sample holder. The thermometer had a resistance of approximately 50 kΩ at 4.2 K and 8 MΩ at 1 K. The power dissipated by polarizing the thermometers was in the range of 10^{-8} W. Analysis of the MTO data was made in two steps. We first obtained a Fourier power spectrum in order to get the dHvA frequencies; then a numerical filter program using the method of Kaiser and Reed[23] allowed us to select the amplitude-versus-field variation of a given dHvA frequency and to obtain the corresponding effective mass. When it was necessary, analog filtering was done before data acquisition. Care was taken to eliminate the effect of unknown heat capacity of the sample holder which is in thermal contact with the sample (e.g., quartz plate, grease, etc.). This was done by dividing the amplitudes at two different magnetic fields at the same temperature. Then the effective masses and the Dingle temperatures were given by the variation of the amplitude ratio with temperature or magnetic field.

IV. EXPERIMENTAL RESULTS

We studied the frequencies, the effective masses, and the Dingle temperature for the c-axis direction. Typical results are shown in Fig, 1 in which parts (a) and (b) represent the MTO observed in a second-stage HNO_3 GAC before and after analog filtering; parts (c) and (d) represent the respective Fourier transforms (FT). The analog filtering allows us to increase the signal-to-noise ratio for the determination of the effective masses. Figure 2 shows the MTO and the corresponding FT for stage 4. The differences from stage 2 are clear.

The dHvA frequencies and the effective masses found are the same for samples of the same stage; however, the Dingle temperature is sample dependent. In Table I we summarize the results obtained for the c-axis direction. The frequencies are between 50 tesla and 1200 tesla and the effective masses are between $0.1m_0$ and $1.5m_0$. The frequencies are measured within 3%. The errors in the determination of the effective masses may be high because of the small amplitudes of the FT relative to the noise and the presence of a great number of dHvA frequencies in a small range. The conclusion of these results is that although they remain in the same range, the frequencies are different from one stage to another.

We were able to study the angular variation of only the lowest frequency of the second stage up to 35° from the c axis. We were limited to 35° since the variation of the mass in this range already divided the signal by 1000 relative to that along the c axis. This brings the FT amplitude to the noise level. This variation which is represented in Fig. 3 fits well with a cylinder, i.e., a 2D Fermi surface. But it should be mentioned that any ellipsoidal FS of anisotropy greater than 10 would fit as well the observed variation, owing to the precision of the measured dHvA frequencies, the latter being limited by the low number of oscillations which has been observed.

Let us now look in more detail at the different stages. For the second stage we have a main frequency α of 235 tesla. The corresponding effective mass is $0.15m_0$. We also observe the harmonics 2α and 3α. The effective mass of the 2α frequency is twice that of the effective mass of the α frequency in agreement with the MTO theory (Sec. III A). All the other frequencies except the frequency at 630 tesla form an arithmetic series

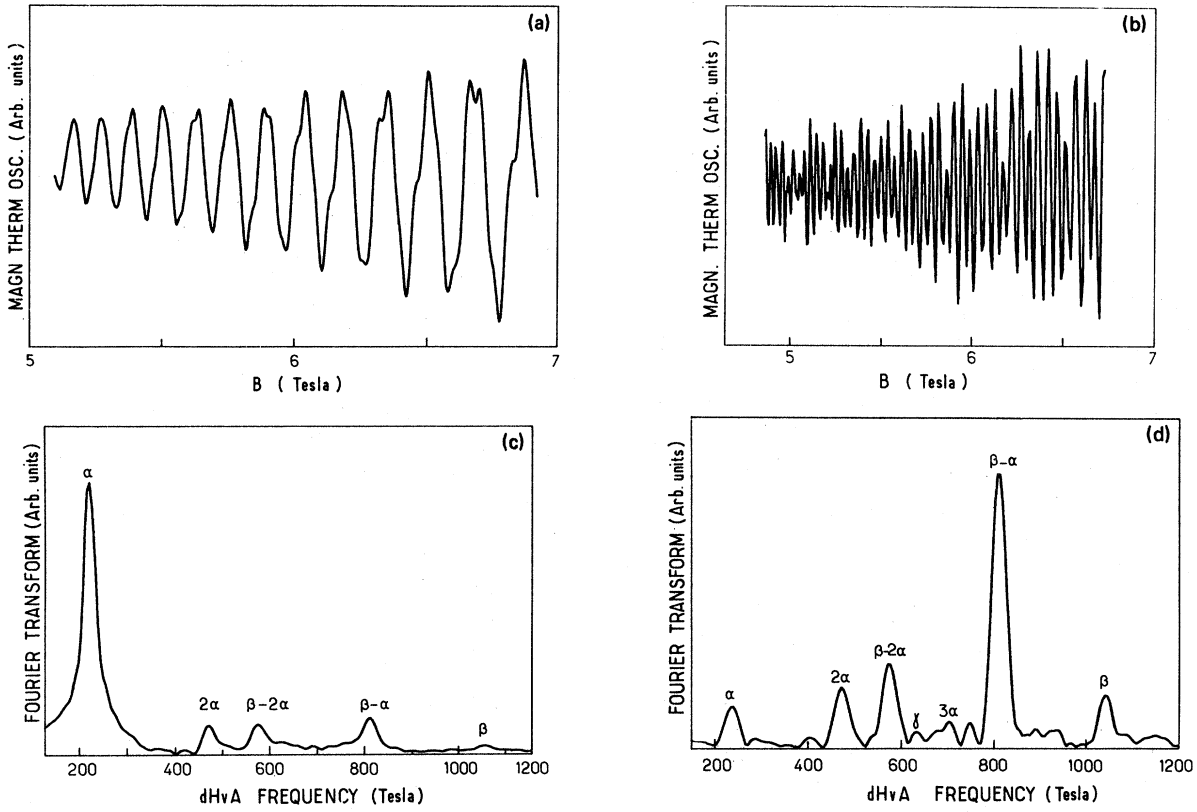

FIG. 1. Typical MTO results for the second-stage HNO_3 GAC: (a) and (b) MTO before (a) and after analog filtering. (c) and (d): the corresponding Fourier transforms [(c) for (a) and (d) for (b)].

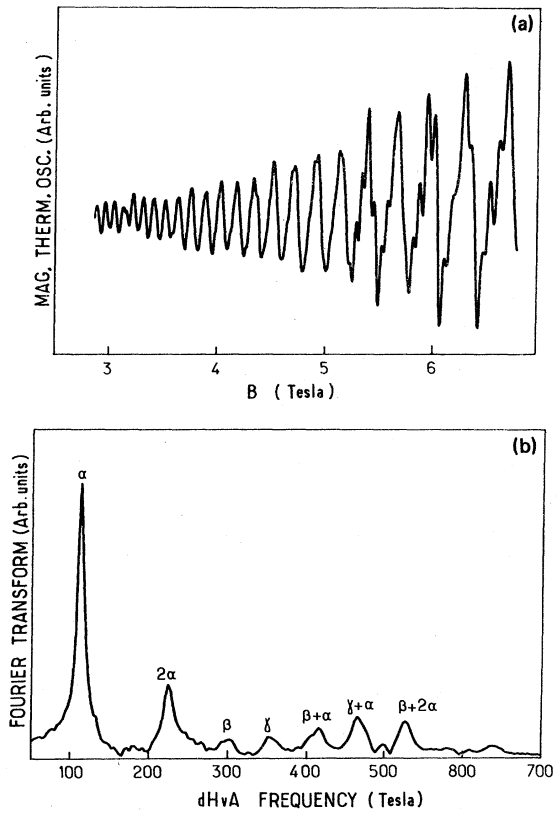

FIG. 2. MTO results for the fourth HNO_3 GAC: (a) MTO and (b) Fourier spectrum.

of argument α.

For the third stage the main frequency, labeled β, is 421 tesla. The corresponding effective mass is $0.37m_0$. We have also observed three other frequencies which form an arithmetic series. The difference between successive terms is the frequency β. There is also an isolated low frequency γ of 40 tesla and its harmonic 2γ.

For the fourth stage the dHvA spectrum is rather complex. The main frequency labeled α is 109 tesla with an effective mass of $0.20m_0$. We have also observed 2α. All the other frequencies can be ordered in two families obtained by adding $n\alpha$ to the fundamental frequencies β and γ of 300 and 351 tesla which have the lowest effective masses: $0.30m_0$ and $0.15m_0$, respectively. The labeling of the frequencies is described below (Sec. V).

We measured Dingle temperatures T_i of some of our samples. We found that T_i for a given sample is the same for all the orbits (within the experimental error) but varies from one sample to another for a given stage. The latter point arises from the fact that the scattering is dominated by static defects at liquid-He temperatures. T_i changes when a given sample is cycled from room temperature to 4.2 K if the temperature is lowered at different rates. This should be associated to the existence of a phase transition in RGN at ~250 K: the intercalate is in a liquid state at room temperature and the crystallization must be made very slowly in order to obtain a good in-plane ordering of the intercalate. Typical results for T_i are between 4 and 12 K.

V. TOPOLOGY OF THE FERMI SURFACE AND MAGNETIC BREAKDOWN

As we mentioned above, a feature of the dHvA spectra common to the three stages which we also observed earlier in the Br_2 GAC (Ref. 6) is the presence of combinations of frequencies by addition or subtraction. We can see, for example, in the second stage the family 335, 570, 805, 1040 which is an arithmetic series of increment 235, precisely the α frequency. This means there exists a coupling mechanism between orbits on the FS. This coupling can be due to magnetic breakdown.[24] This implies that the orbits on the FS are separated by small gaps. With a sufficient magnetic field the electrons can thus jump from one orbit to the other.

TABLE I. MTO results: dHvA frequencies F and relative cyclotron effective masses for stages 2, 3, and 4 of HNO_3 GAC.

Stage 2			Stage 3			Stage 4		
Label	F (tesla)	m^*/m_0	Label	F (tesla)	m^*/m_0	Label	F (tesla)	m^*/m_0
α	235	0.15 ± 0.02	γ	40	<0.05	α	109	0.20 ± 0.05
$\beta-3\alpha$	335	0.8 ± 0.3	2γ	80		2α	219	0.5 ± 0.1
2α	470	0.25 ± 0.05	$\alpha-\beta$	240	0.8 ± 0.1	β	300	0.3 ± 0.1
$\beta-2\alpha$	570	0.5 ± 0.2	β	421	0.37 ± 0.02	γ	351	0.15 ± 0.1
γ	630		α	662	0.25 ± 0.2	$\beta+\alpha$	411	0.5 ± 0.1
3α	705					$\gamma+\alpha$	460	0.3 ± 0.1
$\beta-\alpha$	805	0.3 ± 0.3				$\beta+2\alpha$	521	0.8 ± 0.2
β	1040					$\gamma+2\alpha$	580	
						$\beta+3\alpha$	630	

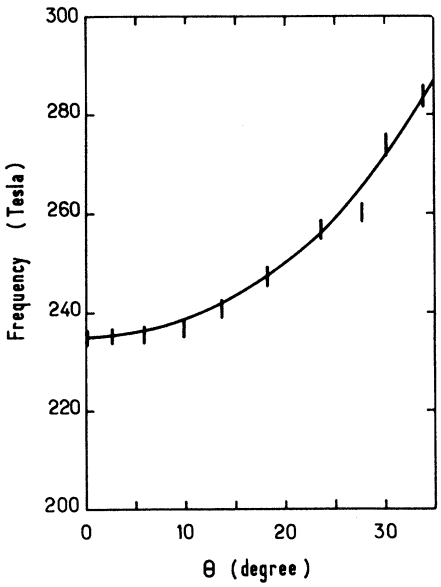

FIG. 3. Angular variation of the α dHvA frequency for the second-stage compound. θ is the angle between the magnetic field and the c axis. The continuous line represents the frequency corresponding to an FS cylindrical along the c axis.

If two orbits are coupled by magnetic breakdown, the resulting dHvA frequency is the addition or subtraction of the frequencies of the two primitive orbits. The frequencies combine by addition if the two orbits have the same character (electron or hole) and combine by subtraction if their characters are opposite. Moreover, in both cases the effective mass is the addition of the effective masses of the two primitive orbits. This allows us to find the primitive orbits and frequencies as those which have the smallest effective masses in the series of frequencies and to correctly label the orbits. At the same time we know the relative character of the primitive frequencies of the series.

In the second-stage compound we have a family with two primitive orbits (α and β) of opposite character and another family made of an isolated orbit γ. In the third stage we also have the same situation with a family with two primitive orbits (α and β) of opposite character and another family with an isolated frequency γ. In the fourth stage we have two families with primitive orbits: α, β and α, γ, respectively. All the observed orbits have the same character. We shall now go to a more detailed interpretation of our experimental results in terms of the electronic band structure and Fermi surface.

VI. ELECTRONIC STRUCTURE OF THE GRAPHITE ACCEPTOR COMPOUNDS

A. The 2D unit zone

The main structural feature of the graphite acceptor compounds is the charge transfer between the intercalate layer and the surrounding carbon layers. This transfer may be characterized by the number of carriers (electrons) accepted by the intercalate and the number of holes left in the carbon layers and their distribution among the different carbon layers.

This transfer results in a charged intercalate layer which contains localized electrons and which acts as an electrostatic screen between the two sides of the intercalate. This is a high potential barrier which prevents the carriers from moving from the zone on one side of the intercalate to the zone at the other side so that the movement of the charge carriers perpendicular to the layer is forbidden. The 2D properties of the GAC have their origin in the presence of these intercalate layers strongly charged with localized electrons. The crystal space is therefore divided along the c direction in 2D unit zones (UZ) bounded by the intercalate layers within which the carriers can move only in the direction parallel to the layers. Such a 2D UZ is made of a sequence of s carbon layers (for stage s) containing delocalized holes; its length in the c direction is the identity period of the GAC. The dynamical properties, e.g., the FS's, which are measured are those of the carriers within a 2D UZ whose electronic structure will be presented now.

B. Band structure of the two-dimensional unit zone

Blinowski *et al.*[10,25] have computed the band structure of the sth stage 2D UZ. They suppose that it is made of s interacting carbon layers differently charged with holes. The intercalate layer is considered as an homogeneous charge distribution of electrons with a density adequate to conserve the neutrality of the 2D UZ. They made explicit calculations for stages 1, 2, 3, and 4.

For the first-stage GAC the 2D UZ contains only one carbon layer, then the approximate dispersion relation,

$$E = \pm \tfrac{3}{2} b \gamma_0 k , \tag{6.1}$$

where b is the distance between the nearest carbon atoms ($b = 1.42$ Å), γ_0 is the resonance integral between the nearest carbon atoms, and k is the momentum vector computed from the U and U' points (the corners of the 2D graphite BZ). The dispersion relation for an isolated carbon layer, i.e., without interaction, is linear in k.

For the second-stage compound there are two carbon layers in interaction. If this interaction is neglected, one obtains the bands of one carbon layer twice degenerate. The interaction splits the degeneracy of the bands. Blinowski *et al.* limit this interaction to γ_1, the resonance integral for the nearest atoms of two layers. The following dispersion relations are found for the four bands, two valence bands, and two conduction bands (Fig. 4):

$$E_{c_1} = -E_{v_1} = \tfrac{1}{2}[(\gamma_1^2 + 9\gamma_0^2 b^2 k^2)^{1/2} - \gamma_1] , \quad (6.2)$$

$$E_{c_2} = -E_{v_2} = \tfrac{1}{2}[(\gamma_1^2 + 9\gamma_0^2 b^2 k^2)^{1/2} + \gamma_1] . \quad (6.3)$$

The two parameters γ_0 and γ_1 depend on the charge-transfer coefficient and on the spatial distribution of the excess charge. Blinowski *et al.*[10] estimate that their numerical value will not be very different from that of pristine graphite.[26] We will discuss this later (Sec. VII) in connection with the interpretation of our results. Usually $|E_F| > \gamma_1$ so that the FS is made of two circles of radii k_{F_1} and k_{F_2} centered around U and U'.

Blinowski and Rigaux[25] (BR) also computed the band structure of the third stage. In this stage there are three interacting carbon layers differently charged: two are external and one is an internal layer. Let 2ϵ be the electrostatic potential-energy difference between an external and an internal layer, due to the difference in charge. In their calculation BR also limited the interaction between the layers to the γ_1 parameter and have obtained an analytical expression for the bands. If one neglects γ_1, one obtains the linear band structure of Fig. 5. In this case the bands relative to the external layers are twice degenerate and shifted up by 2ϵ relative to the bands of the internal layers.

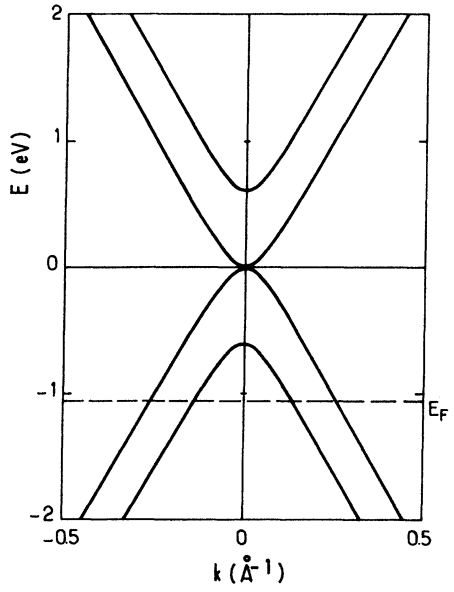

FIG. 4. Bands for the second-stage HNO_3 GAC within the Blinowski-Rigaux model. The values of the two γ parameters are $\gamma_0 = 2.40$ eV and $\gamma_1 = 0.61$ eV.

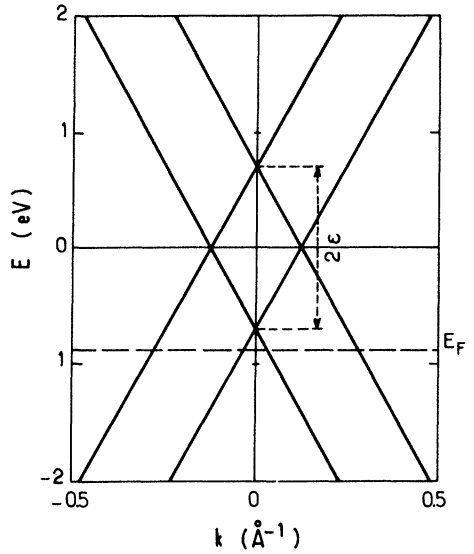

FIG. 5. Linear approximation for the bands in the third stage. The bands corresponding to the internal layer are shifted down rigidly from the bands corresponding to the external layers by 2ϵ. The values of the parameters are $2\epsilon = 1.4$ eV and $\gamma_0 = 2.40$ eV.

BR made also an explicit calculation for the fourth stage. Here also if γ_1 is neglected, one obtains the system of linear bands of Fig. 5, except that all the bands are here twice degenerate. It should be mentioned that far from the crossover the bands are almost linear in all the stages even if the γ_1 interaction is taken into account.

C. Effect of the in-plane order of the intercalate

In the computation of Blinowski *et al.*[10,25] the intercalate layer is considered simply as a homogeneous distribution of negative charge, the only requirement being the overall neutrality of the 2D UZ and hence of the GAC. Actually the molecules of the intercalate layer are ordered, at least at low temperature. Thus the charge of the electrons localized on the intercalate molecules sites is no longer homogeneously distributed, but varies with the periodicity of the intercalate lattice. This results in a new periodic potential which is seen by the delocalized holes in the graphite layers and produces a new periodicity in the band structure of the GAC.

As a result, energy gaps appear at the Bragg diffraction planes, defined[27] by the equation

$$\{\vec{k}\} = \{\vec{k} + l\vec{G} + m\vec{q}\}. \quad (6.4)$$

In this equation $\{\vec{k}\}$ is the star of the $\vec{k}$ vector according to the symmetry of the compound, $\vec{G}$ and $\vec{q}$ are the 2D basic reciprocal-lattice vectors corresponding to the carbon layer and the intercalate layer, and l and m are arbitrary integers. This equation has many more solutions than the corresponding equation for the simple 2D graphite lattice

$$\{\vec{k}\} = \{\vec{k} + l\vec{G}\}. \quad (6.5)$$

Consequently, new energy gaps appear which modify the topology of the FS of the GAC relative to that of pristine 2D graphite.

For the construction of the actual FS of the 2D UZ we proceed in the following way. We begin by constructing, in the extended-zone scheme of the 2D graphite BZ, the isoenergy surfaces for $E = E_F$ as given by the BR model. These are circles centered around the different U and U' points. To these circles we apply the translations $m\vec{q}$ to bring back these circles into a single BZ. The actual FS is made of the different pieces resulting from the intersections of all these circles. It should be mentioned that this construction is valid in all the cases, whether the intercalate and graphite lattices are commensurate or not. In the commensurate case, i.e., when $\vec{q} = (l/m)\vec{G}$, it is possible to define a new basic periodicity which includes both the 2D graphite and the intercalate lattice periodicities. In this case we obtain the FS by folding the isoenergy circles of the 2D graphite BZ in the intercalate BZ, which is $(l/m)^2$ times smaller. This kind of construction is a particular case of the general one described above.

VII. INTERPRETATION OF THE SECOND-STAGE RESULTS

A. Crystallographic structure

We do not know the exact crystallographic structure of the HNO_3 intercalate layer. However, we are able to determine it by imposing agreement between the FS obtained for a given crystallographic structure and that obtained from our experimental MTO results. At least, at sufficiently low temperature it is expected that the intercalate lattice will be commensurate with the graphite lattice, so that we shall consider the commensurate case. The chemical composition is $C_{16}(HNO_3)$. We assume a hexagonal unit cell for the intercalate. As we shall see below this assumption explains very well our experimental results. If N is the number of molecules per unit cell the possible cells which give an intercalate lattice commensurate with the graphite lattice will contain $N = 1, 3, 4, 9, 12, 16, \ldots$ molecules. The only hexagonal unit cell commensurate with the graphite lattice which gives agreement with our experimental results is a unit cell containing four acid molecules and is 16 times larger than that of graphite. The primitive vectors of this lattice are parallel to those of the graphite lattice and are four times larger ($4a \times 4a$). The side of this cell is $a = 5.68$ Å $= 4b$ and the area $S = 83.83$ Å^2. The corresponding BZ is also hexagonal with a side of $G = 0.426$ Å^{-1} and an area of $\Omega = 0.47$ Å^{-2}.

B. The Fermi surface

According to the model of Blinowski and Rigaux the isoenergy surfaces are two circles around the U and U' points of the 2D graphite BZ. By folding these surfaces in the BZ of the 2D UZ, the U and U' points of the 2D graphite BZ are superimposed on the U and U' points of the 2D UZ BZ. The isoenergy surfaces are circles around the U and U' points of the new BZ.

As we see in Fig. 6, if we impose agreement with the main frequency α, $F_\alpha = 235$ tesla, we obtain for the second main frequency β, $F_\beta = 1014$ tesla. This frequency corresponds to a star with six branches and is found, according to our experimental results to be 1040 tesla. The agreement between these values is good. All the other frequencies of this set are obtained as combinations by magnetic breakdown of these two basic frequencies. This implies a Fermi momentum $k_{F_1} = 0.265$ Å^{-1} which is the radius of the largest FS circle. The second set includes only the γ frequency $F_\gamma = 630$ tesla. This value implies for the second Fermi momentum $k_{F_2} = 0.138$ Å^{-1}.

The topology of the FS (Fig. 6) imposes the conditions $k_{F_1} + k_{F_2} < G$, $2k_{F_1} > G$ which are indeed verified.

From our results we get the two Fermi momenta k_{F_1} and k_{F_2}. These two values coupled with the dispersion relations given by the BR model allow

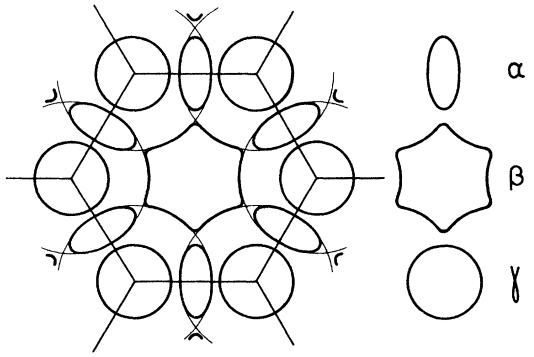

FIG. 6. Brillouin zone and Fermi surface for the second-stage HNO_3 GAC. The three basic frequencies α, β, and γ are shown aside from the Brillouin zone.

us to determine many physical quantities: the charge-transfer factor f, the Fermi energy E_F relative to the crossing of the 2D graphite bands, and the band mass for every orbit.

For f we find the expression

$$f=\frac{3\sqrt{3}}{4\pi} lb^2(k_{F_1}^2+k_{F_2}^2), \tag{7.1}$$

where l is the number of carbon atoms per intercalate molecule and per carbon layer (here $l=8$). f, which is associated to the total number of free carriers, is independent of the γ_0 and γ_1 parameters. E_F is given by

$$E_F=\frac{3b}{2\sqrt{2}}\gamma_0(k_{F_1}^2+k_{F_2}^2)^{1/2}. \tag{7.2}$$

The band mass is defined by the general relation

$$m^b=\frac{\hbar^2}{2\pi}\frac{\partial A}{\partial E}\bigg|_{E=E_F}.$$

We obtain, respectively, for the three basic masses

$$m_\alpha^b=-\frac{4\hbar^2(\gamma_1^2+9\gamma_0^2b^2k_{F_1}^2)^{1/2}}{9\pi\gamma_0^2b^2}\arccos\frac{G}{2k_{F_1}}, \tag{7.3}$$

$$m_\beta^b=-\frac{4\hbar^2(\gamma_1^2+9\gamma_0^2b^2k_{F_1}^2)^{1/2}}{9\pi\gamma_0^2b^2}\left(\pi-3\arccos\frac{G}{2k_{F_1}}\right), \tag{7.4}$$

$$m_\gamma^b=-\frac{2\hbar^2(\gamma_1^2+9\gamma_0^2b^2k_{F_2}^2)^{1/2}}{9\gamma_0^2b^2}. \tag{7.5}$$

The two γ parameters obtained in this way are not independent. They are related by the expression

$$\frac{\gamma_0}{\gamma_1}=\frac{2\sqrt{2}}{3b}\frac{(k_{F_1}^2+k_{F_2}^2)^{1/2}}{k_{F_1}^2-k_{F_2}^2} \tag{7.6}$$

which gives

$$\gamma_0=3.86\gamma_1.$$

Thus by fixing only one γ parameter we obtain the values of the Fermi energy and the band masses.

The only estimate of these parameters for GAC was made by Blinowski *et al.*[10] They take 2.40 eV for γ_0. With this value the band structure of the 2D graphite along the U-W line is in fairly good agreement with that obtained by more general calculations. They interpret the minimum observed at 0.37 eV in the reflectivity spectrum of the second-stage GAC as due to an interband transition between the two valence bands (see Fig. 4). According to their model this transition gives directly γ_1.

Once the Fermi momenta k_{F_1} and k_{F_2} are given, the parameters γ_0 and γ_1 are related by Eq. (7.6). If we choose $\gamma_0=2.40$ eV, we get $\gamma_1=0.62$ eV, but if we choose $\gamma_1=0.37$ eV, we get $\gamma_0=1.43$ eV. In the first two columns of Table II we summarize the results obtained for the transfer factor, the Fermi energy, and the band masses by using Eqs. (7.1) to (7.6) with the two choices of γ parameters. The cyclotron mass (m^*) and the corresponding band mass (m^b) are related by

$$m^*=m^b(1+\lambda),$$

where $\lambda>0$ is the many-body mass-enhancement constant mainly due to electron-phonon coupling. Hence the observed cyclotron masses give an upper limit for the band masses and this in turn gives a lower limit of 2.40 eV for γ_0. We take this value for γ_0. The resulting numerical values for the physical quantities are represented in the second column of Table II. We obtain for the charge-transfer factor $f=0.6$. This value is independent of the γ_0 and γ_1 choice, as we determine the f factor in a direct way from the number of free carriers in the graphite layers. The Fermi energy is $E_F=-1.08$ eV. This value depends on γ_1.

TABLE II. Parameters for the second-stage compounds. Upper part: reciprocal-lattice vector and Fermi radii; lower part: results for different choices of γ parameters.

$G=0.426$ Å^{-1} $K_{F_1}=0.265$ Å^{-1} $K_{F_2}=0.138$ Å^{-1}		
$\gamma_0=1.43$ eV	$\gamma_0=2.40$ eV	$\gamma_0=2.40$ eV
$\gamma_1=0.37$ eV	$\gamma_1=0.62$ eV	$\gamma_1=0.50$ eV
		$\gamma_3=0$
		$\gamma_4=0.15$ eV
$f=0.60$	$f=0.60$	$f=0.60$
$E_F=-0.65$ eV	$E_F=-1.08$ eV	$E_F=-1.03$ eV
$m_\alpha^b=-0.28m_0$	$m_\alpha^b=-0.16m_0$	$m_\alpha^b=-0.17m_0$
$m_\beta^b=0.53m_0$	$m_\beta^b=0.32m_0$	$m_\beta^b=0.33m_0$
$m_\gamma^b=-0.38m_0$	$m_\gamma=-0.22m_0$	$m_\gamma^b=-0.20m_0$

Some other estimates of these values for second-stage compounds have been made. Weinberger *et al.*[9] have obtained from electron paramagnetic resonance studies the density of states at the Fermi level for the AsF_5 GAC. They interpret these results by considering the second-stage GAC as two independent graphite layers. This gives $f=0.48$ and $E_F=-1.14$ eV in good agreement with our values. Blinowski *et al.*,[10] by combining reflectivity experiments with their theoretical model, find, for different second stages, GAC values of f between 0.25 and 0.51 (taking $\gamma_0=2.40$ eV) and E_F between -0.7 and -1 eV.

For pure graphite and in the framework of the

Slonczewski-Weiss model which includes several additional parameters, γ_1 can be inferred from the effective masses of the carriers. The estimated value is ~0.40 eV.[26] γ_0 is chosen to fit all the data. From the analysis of carriers on the Fermi level γ_0 was estimated at ~3.20 eV. This γ_0 value explains well the observed physical quantities for pure graphite. In GAC we are far away from the Fermi level of pure graphite and for the BR model the value of 2.40 eV is the best adapted.

From our results we find $\gamma_1 = 0.62$ eV. This value is different from the direct estimate, $\gamma_1 = 0.37$ eV, of Blinowski *et al.*[10] from the reflectivity. We think that the difference is due to the fact that in the BR model the interaction between adjacent carbon layers is described only by the γ_1 parameter. Moreover, in the Slonczewski-Weiss model this is described by three parameters γ_1, γ_3, and γ_4. The value of $\gamma_1 = 0.62$ eV that we find within the BR model may be some kind of total interaction between adjacent carbon layers. To look into this idea more in detail we generalize the BR model by including the other parameters describing the interaction between adjacent carbon layers.

C. Extension of the Blinowski-Rigaux model

There is a discrepancy in the γ_1 values between the direct estimation from optical reflectivity of Blinowski *et al.*[10] and the value inferred from our results. For pure graphite, McClure[28] has shown that all the experiments can be explained within the Slonczewski-Weiss model with seven parameters. In particular, the interaction between two adjacent layers is described by three parameters γ_1, γ_3, and γ_4.

We can extend the Blinowski-Rigaux model by introducing other overlap parameters, namely, γ_3 and γ_4. The Hamiltonian is then

$$\mathcal{H} = \begin{pmatrix} 0 & \gamma_1 & -\gamma_0 g_0^* & \gamma_4 g_0 \\ \gamma_1 & 0 & \gamma_4 g_0^* & -\gamma_0 g_0 \\ -\gamma_0 g_0 & \gamma_4 g_0 & 0 & \gamma_3 g_0^* \\ \gamma_4 g_0^* & -\gamma_0 g_0^* & \gamma_3 g_0 & 0 \end{pmatrix}, \tag{7.7}$$

where $g_0(\vec{k})$ can be written in polar coordinates as

$$g_0(k,\alpha) = \exp(ibk\sin\alpha) + 2\exp\left(\frac{-ibk\sin\alpha}{2}\right)\cos\left(\frac{\sqrt{3}\,bk\cos\alpha}{2} - \frac{2\pi}{3}\right). \tag{7.8}$$

k is the length of the wave vector with U as origin and α is the polar angle as specified in Fig. 7. We obtain the analytical expressions resulting from the diagonalization of this Hamiltonian in two particular cases:

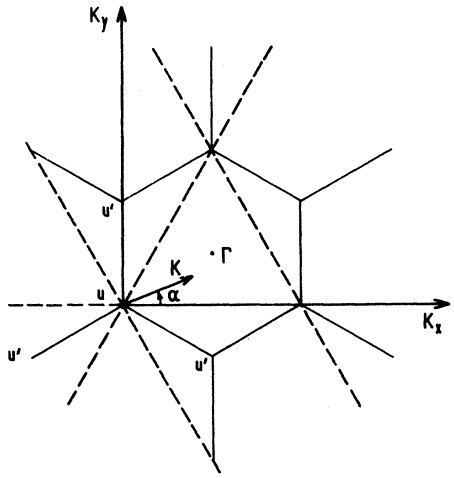

FIG. 7. This figure defines the coordinate system for the wave vector in the BZ of the GAC. The U point is taken as origin and α is the polar angle relative to the k_x direction. The U' point has a threefold symmetry relative to U. The dashed lines correspond to the angle $\alpha = n\pi/3$ where an explicit analytical solution for the general secular equation including the γ_3 parameter can be found.

(1) $\alpha = n\pi/3$, which implies $g_0(k,\alpha)$ real. We obtain the following dispersion relations (Fig. 8):

$$E_{c_2}(k, n\pi/3) = \tfrac{1}{2}\{[(\gamma_1 - \gamma_3 g_0)^2 + 4g_0^2(\gamma_0 - \gamma_4)^2]^{1/2} - \gamma_1 + \gamma_3 g_0\}, \tag{7.9}$$

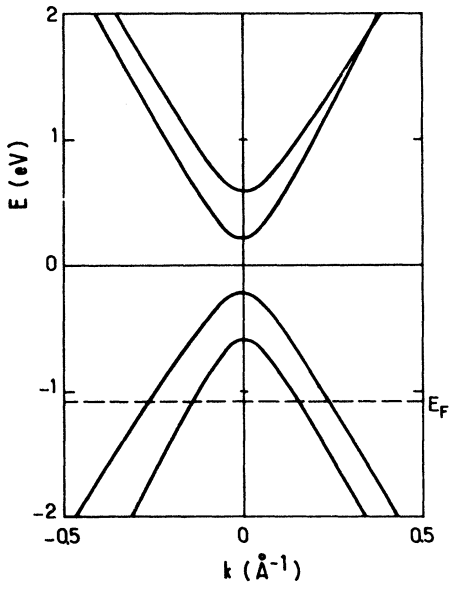

FIG. 8. Bands of the second-stage compound along the direction $\alpha = n\pi/3$ where an explicit analytical solution can be found. The numerical value of the parameters are $\gamma_0 = 2.40$ eV, $\gamma_1 = 0.37$ eV, $\gamma_3 = 0.20$ eV, and $\gamma_4 = 0.15$ eV.

$$E_{c_1}(k, n\pi/3) = \tfrac{1}{2}\{[(\gamma_1 - \gamma_3 g_0)^2 + 4g_0^2(\gamma_0 + \gamma_4)^2]^{1/2} - \gamma_1 - \gamma_3 g_0\}, \quad (7.10)$$

$$E_{v_1}(k, n\pi/3) = -\tfrac{1}{2}\{[(\gamma_1 - \gamma_3 g_0)^2 + 4g_0^2(\gamma_0 - \gamma_4)^2]^{1/2} - \gamma_1 - \gamma_3 g_0\}, \quad (7.11)$$

$$E_{v_2}(k, n\pi/3) = -\tfrac{1}{2}\{[(\gamma_1 - \gamma_3 g_0)^2 + 4g_0^2(\gamma_0 + \gamma_4)^2]^{1/2} + \gamma_1 + \gamma_3 g_0\}. \quad (7.12)$$

There are four bands: two of valence and two of conduction. In this case

$$g_0\left(k, n\frac{\pi}{3}\right) = \cos\left(\frac{bk\sqrt{3}}{2}\right)\left\{1 + 2\cos\left[\frac{bk\sqrt{3}}{2}\cos\left(\frac{n\pi}{3}\right) - \frac{2\pi}{3}\right]\right\}. \quad (7.13)$$

Here the isoenergy surfaces are not circles but warped surfaces of hexagonal symmetry centered around U and U'. These dispersion relations cannot be compared in a simple way with the experimental data on the FS, which give the whole FS area in the layer plane. The approximation consisting of a circular FS with the radius corresponding to the value given by $\alpha = n\pi/3$ is of the same order as that which neglects γ_3.

(2) If $\gamma_3 = 0$. We obtain (Fig. 9):

$$E_{c_2}(k) = \tfrac{1}{2}\{[\gamma_1^2 + 4|g_0|^2(\gamma_0 - \gamma_4)^2]^{1/2} + \gamma_1\}, \quad (7.14)$$

$$E_{c_1}(k) = \tfrac{1}{2}\{[\gamma_1^2 + 4|g_0|^2(\gamma_0 + \gamma_4)^2]^{1/2} - \gamma_1\}, \quad (7.15)$$

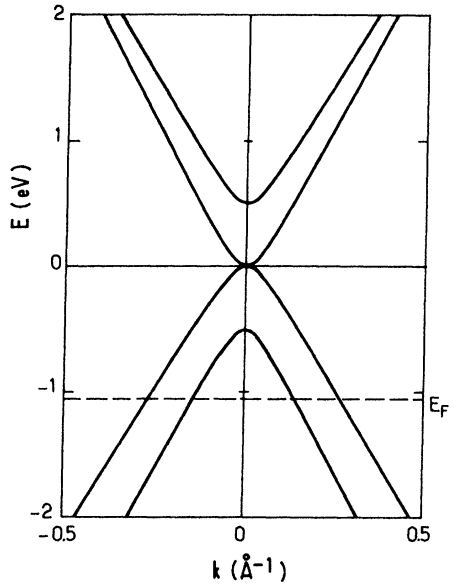

FIG. 9. Bands for the second stage, when γ_3 is neglected. The value of the parameters are $\gamma_0 = 2.40$ eV, $\gamma_1 = 0.50$ eV, and $\gamma_4 = 0.15$ eV.

$$E_{v_1}(k) = -\tfrac{1}{2}\{[\gamma_1^2 + 4|g_0|^2(\gamma_0 - \gamma_4)^2]^{1/2} - \gamma_1\}, \quad (7.16)$$

$$E_{v_2}(k) = -\tfrac{1}{2}\{[\gamma_1^2 + 4|g_0|^2(\gamma_0 + \gamma_4)^2]^{1/2} + \gamma_1\}. \quad (7.17)$$

If we develop $g_0(k, \alpha)$ for small k's ($k < G$), we obtain

$$|g_0(k)| = \tfrac{3}{2}bk \quad (7.18)$$

which is the value used for pure graphite. For intercalation compounds this expression should remain valid, but it must be tested in every case. The general $g_0(k, \alpha)$ expression introduces an additional warping in the FS, but this warping is less than $\frac{1}{10}$ of that introduced by γ_3. Now the FS is made of two circles ($|E_F| > \gamma_1$) centered around the U and U' points of the BZ, and we can compare this with our experimental results.

We find the following expressions for the Fermi energy and the effective masses:

$$E_F = -\frac{3b}{2\sqrt{2}}[(\gamma_0 - \gamma_4)^2 k_{F_1}^2 + (\gamma_0 + \gamma_4)^2 k_{F_2}^2]^{1/2}, \quad (7.19)$$

$$m_\alpha = -\frac{4\hbar^2[\gamma_1^2 + 9b^2(\gamma_0 - \gamma_4)^2 k_{F_1}^2]^{1/2}}{9\pi b^2(\gamma_0 - \gamma_4)^2}\arccos\frac{G}{2k_{F_1}}, \quad (7.20)$$

$$m_\beta = -\frac{4\hbar^2[\gamma_1^2 + 9b^2(\gamma_0 - \gamma_4)^2 k_{F_1}^2]^{1/2}}{9\pi b^2(\gamma_0 - \gamma_4)^2} \times \left(\pi - 3\arccos\frac{G}{2k_{F_1}}\right), \quad (7.21)$$

$$m_\gamma = -\frac{2\hbar^2[\gamma_1^2 + 9b^2(\gamma_0 + \gamma_4)^2 k_{F_2}^2]^{1/2}}{9b^2(\gamma_0 + \gamma_4)^2}. \quad (7.22)$$

Since we know k_{F_1} and k_{F_2}, we have the following relation between the three parameters:

$$\gamma_1^2 = \frac{9b^2}{8}\frac{[(\gamma_0 - \gamma_4)^2 k_{F_1}^2 - (\gamma_0 + \gamma_4)^2 k_{F_2}^2]^2}{(\gamma_0 - \gamma_4)^2 k_{F_1}^2 + (\gamma_0 + \gamma_4)^2 k_{F_2}^2}. \quad (7.23)$$

Of the three γ parameters, two are independent. Like Blinowski *et al.* we take $\gamma_0 = 2.40$ eV. The best choice of the two other band parameters to agree with our experimental results for k_{F_1}, k_{F_2}, and the effective masses is $\gamma_1 = 0.50$ eV and $\gamma_4 = 0.15$ eV. In the third column of Table II we summarize the results obtained with these parameters. It should be mentioned that the physical quantities related to the density of states at the Fermi level (effective masses, transfer ratio, Fermi level) are almost insensitive to the values of γ_1 and γ_4 and depend only on γ_0.

If we attribute the minimum observed[10] at 0.37 eV in the optical reflectivity to an interband transition between the two valence bands, the energy of this transition is

$$\Delta E_v = \gamma_1 + \tfrac{1}{2}\{[\gamma_1^2 + 9b^2(\gamma_0+\gamma_4)^2k^2]^{1/2} - [\gamma_1^2 + 9b^2(\gamma_0-\gamma_4)^2k^2]^{1/2}\}. \quad (7.24)$$

If we take the previous values of γ_0, γ_1, and γ_4 we get $\Delta E_v = 0.63$ eV, which is too large. Once γ_0 is fixed at 2.40 eV, the value of ΔE_v is almost independent of γ_1 [γ_4 is given by (7.23)]. If the value of ΔE_v is increased (2.40 eV is the lowest possible limit), ΔE_v is even larger. In any case the agreement with the experimental value of 0.37 eV is very poor.

In order to explain this optical transition and our results together, we must introduce in the BR model the γ_3 and γ_4 parameters. If we take for γ_1, γ_3, and γ_4 the usual values of pure graphite we find for the optical transition an energy $\Delta E_v \sim 0.42$ eV. But this value is an average value and must be taken cautiously. A full computer calculation should be done to confirm this last point.

VIII. INTERPRETATION OF THE RESULTS FOR THE THIRD- AND FOURTH-STAGE COMPOUNDS

A. Third stage

The electronic structure of the third stage is more complex than that of the second stage owing to the presence of the electrostatic energy difference 2ϵ and the existence of six bands instead of four. We are not able to interpret our results in a way as satisfactory as for the second stage owing to their less complete character and to the complexity of the bands. Nevertheless, we will try to understand them by making some approximations. We neglect the interaction between the layers. Then the bands are those given in Fig. 5, where the lowest band corresponds to the internal carbon layer and the highest, twice degenerate, to the external ones. We suppose that the in-plane order is here the same as in the second stage. We attribute the smallest and isolated γ dHvA frequency to a Fermi circle originated by the band corresponding to the internal carbon layer; this gives $k_{F_1} = 0.035$ Å^{-1}. The remaining α and β dHvA frequencies are attributed to a Fermi circle of the external layer. Following the procedure described in Sec. VII B for folding the 2D graphite BZ in the 2D unit zone BZ, we find an FS made of two primitive orbits as represented in Fig. 6. If we impose for the β frequency the experimental value of 421 tesla we find for the second orbit α a frequency of 720 tesla which is in relatively good agreement with the experimental value of 680 tesla. This gives a Fermi radius $k_{F_2} = 0.31$ Å^{-1}. The β-α dHvA frequency results from the magnetic breakdown between the two basic orbits α and β as can be seen also from the relative values of the cyclotron masses. We obtain a reasonable estimate of the electrostatic energy difference 2ϵ between the internal and external carbon layers by using the dispersion relations of the linear bands of Fig. 5. This gives

$$2\epsilon = \tfrac{3}{2} b\gamma_0 (k_{F_2} - k_{F_1}). \quad (8.1)$$

If we take, as for the second stage, $\gamma_0 = 2.40$ eV we find $\epsilon = 0.70$ eV. The Fermi energy is

$$E_F = -(\epsilon + \tfrac{3}{2}\gamma_0 b k_{F_1}) \quad (8.2)$$

which gives $E_F = -0.88$ eV. In this case we find that 99% of the excess charge is localized in the two external layers. We compare now the values of the observed effective masses (m_{expt}) with those computed from the linear bands (m^b) and given by the expressions

$$m_\alpha^b = -\frac{4\hbar^2 k_{F_2}^2}{3\pi b\gamma_0} \arccos\frac{G}{2k_{F_2}}, \quad (8.3)$$

$$m_\beta^b = -\frac{4\hbar^2 k_{F_2}}{3\pi b\gamma_0}\left(\pi - 3\arccos\frac{G}{2k_{F_2}}\right), \quad (8.4)$$

$$m_\gamma^b = -\frac{2\hbar^2 k_{F_1}}{3b\gamma_0}. \quad (8.5)$$

The computed values are given in Table III. We can see a qualitative agreement between m^b and m^*. However, this should be taken with caution.

B. Fourth stage

Our results show that all the orbits have the same character. This is clear from the combination frequencies which are the sum and not the difference frequencies as results from the values of the cyclotron masses observed. However, we are not able to interpret our results in more detail. Indeed, the same character of all orbits seems incompatible with a commensurate unit cell. Studies on the crystallographic structure will hopefully elucidate this point.

IX. CONCLUSION

We have made a detailed study of the Fermi surface and the electronic structure of low-stage ($s = 2, 3, 4$) graphite acceptor compounds. We have used a very stable compound: the residual graphite

TABLE III. Computed band masses for stage 3.

$G = 0.426$ Å^{-1}
$k_{F_1} = 0.035$ Å^{-1}
$k_{F_2} = 0.310$ Å^{-1}
$m^b = -0.24 m_0$
$m^b = 0.19 m_0$
$m^b = -0.05 m_0$

nitrate of formula C_{8s} (HNO_3). We have measured, mainly in the layer plane, the dHvA frequencies, the effective masses, and the Dingle temperatures by using the quantum magnetothermal oscillations. Unlike in the dilute compounds, here the frequency spectrum is different for every stage, an indication of different electronic structures. Combination of frequencies are present in every case and are attributed to the magnetic breakdown resulting from the intersection of the semiclassical orbits.

In order to interpret our results we have used the independent-zones model of the graphite acceptor compounds which considers the compound as a succession of two-dimensional unit zones limited by the intercalate layers. We have compared our results with the band structure of this model computed by Blinowski and Rigaux. For the second stage the Fermi surface and the effective masses agree quantitatively with their computed values, if we fold the bands in the Brilluoin zone of the intercalate. We obtain numerical values for the γ_0 and γ_1 parameters. We have extended the computation by introducing also the γ_3 and γ_4 parameters. We find a charge-transfer ratio $f=0.6$ and a Fermi-level shift of 1.08 eV. For the third stage our results are tentatively interpreted within the linear bands approximation. This gives an estimate of the electrostatic energy difference between the external and the internal carbon layers: $2\epsilon=1.4$ eV. However, all our interpretations are based on a crystallographic structure inferred from our experiments, due to the lack of direct determination. In conclusion, quantum magnetothermal oscillations give valuable results not only on the Fermi-surface properties but also on the band parameters, the charge transfer, and distribution among the different carbon layers in the graphite acceptor compounds.

ACKNOWLEDGMENTS

We are grateful to R. M. Defourneau, R. Leleu, J. Monge, B. Delmas, and G. Genin for technical assistance. We are indebted to C. Rigaux, J. Bok, and J. Blinowski for helpful discussions. Dr. A. W. Moore of the Union Carbide Corporation has kindly supplied us with the HOPG samples. This work was done with the partial support of the Délégation Générale à la Recherche Scientifique et Technique, France, under Grant No. DIF/CCM/79.7.0729.

---

*Laboratoire associé au CNRS.

[1]J. E. Fischer, T. E. Thompson, G. M. T. Foley, D. Guérard, M. Hoke, and F. L. Lederman, Phys. Rev. Lett. 37, 769 (1976).

[2]A. R. Ubbelohde, Proc. R. Soc. London, Ser. A 309, 287 (1968).

[3]L. A. Pendrys, T. C. Wu, C. Zeller, H. Fuzellier, and F. L. Vogel, in proceedings of the 14th Biennial Conference on Carbon, The Pennsylvania State University, University Park, Penn., 1979 (unpublished).

[4]V. F. Gantmakher and V. T. Dologopolov, Zh. Eksp. Teor. Fiz. 60, 2260 (1971) [Sov. Phys.—JETP 33, 1215 (1971)].

[5]F. Batallan, J. Bok, I. Rosenman, and J. Melin, Phys. Rev. Lett. 41, 330 (1978).

[6]I. Rosenman, F. Batallan, and G. Furdin, Phys. Rev. B 20, 2373 (1979).

[7]G. M. T. Foley, C. Zeller, E. R. Falardeau, and F. L. Vogel, Solid State Commun. 24, 371 (1977).

[8]G. Dresselhaus and M. S. Dresselhaus, Mater. Sci. Eng. 31, 235 (1977).

[9]B. R. Weinberger, J. Kaufer, A. J. Heeger, J. E. Fischer, M. Moran, and N. A. W. Holzwarth, Phys. Rev. Lett. 41, 1417 (1978).

[10]J. Blinowski, Nguyen Hy Hau, C. Rigaux, J. P. Vieren, R. Le Toulec, G. Furdin, A. Herold, and J. Melin, J. Phys. (Paris) 41, 47 (1980).

[11]M. S. Dresselhaus, G. Dresselhaus, and J. E. Fischer, Phys. Rev. B 15, 3180 (1977).

[12]I. L. Spain and D. J. Nagel, Mater. Sci. Eng. 31, 183 (1977).

[13]L. Pietronero, S. Strässler, H. R. Zeller, and M. J. Rice, Phys. Rev. Lett. 41, 763 (1978).

[14]C. C. Shieh, R. L. Schmidt, and J. E. Fischer, in Extended Abstracts of the 14th Biennial Conference on Carbon, The Pennsylvania State University, University Park, Pa., 1979.

[15]T. M. Rice and G. K. Scott, Phys. Rev. Lett. 35, 120 (1975).

[16]H. Fuzellier, J. Melin, and A. Herold, Mater. Sci. Eng. 31, 91 (1977).

[17]F. Batallan, J. Bok, I. Rosenman, C. Simon, G. Furdin, H. Fuzellier, and J. Melin, in Extended Abstracts of the 14th Biennial Conference on Carbon, The Pennsylvania State University, University Park, Penn., 1979.

[18]F. Batallan, I. Rosenman, C. Simon, G. Furdin, and H. Fuzellier, in the Proceedings of the International Conference on Layered Materials and Intercalates, Nijmegen, The Netherlands, 1979 [Physica (Utrecht) 99B, 411 (1980)].

[19]A. V. Gold in *Electrons in Metals*, Solid State Physics, edited by J. F. Cochran and R. R. Haering, (Gordon and Breach, New York, 1968), Vol. I, Chap. 2.

[20]A. Goldstein, S. J. Williamson, and S. Foner, Rev. Sci. Instrum. 36, 1356 (1965).

[21]B. McCombe and G. Seidel, Phys. Rev. 155, 633 (1967).

[22]Voltalef grease 901, Prolabo C°, Paris, France.

[23]J. F. Kaiser and W. A. Reed, Rev. Sci. Instrum. 49, 1103 (1978).

[24]R. W. Stark and L. M. Falicov in *Progress in Low Temperature Physics*, edited by C. J. Gorter (North-Holland, Amsterdam, 1967), Vol. 5, Chap. 6.

[25]J. Blinowski and C. Rigaux, J. Phys. (Paris) 41, 667

(1980).
[26]R. O. Dillon, I. L. Spain, and J. W. McClure, J. Phys. Chem. Solids 38, 635 (1977).
[27]L. M. Falicov and M. J. Zuckermann, Phys. Rev. 160, 372 (1967).
[28]J. W. McClure, Phys. Rev. 119, 606 (1960).